MATADOR 2002: A pilot field experiment on convective plumes and dust devils

Nilton O. Renno,[1] Vincent J. Abreu,[1] Jacquelin Koch,[1] Peter H. Smith,[2] Oscar K. Hartogensis,[3] Henk A. R. De Bruin,[3] Dirk Burose,[3] Gregory T. Delory,[4] William M. Farrell,[5] Christopher J. Watts,[6] Jaime Garatuza,[7] Michael Parker,[8] and Allan Carswell[9]

Received 25 November 2003; revised 16 March 2004; accepted 1 April 2004; published 7 July 2004.

[1] Recent research suggests that mineral dust plays an important role in terrestrial weather and climate, not only by altering the atmospheric radiation budget, but also by affecting cloud microphysics and optical properties. In addition, dust transport and related Aeolian processes have been substantially modifying the surface of Mars. Dusty convective plumes and dust devils are frequently observed in terrestrial deserts and are ubiquitous features of the Martian landscape. There is evidence that they are important sources of atmospheric dust on both planets. Many studies have shown that on a small scale, dust sourcing is sensitive to a large number of factors, such as soil cover, physical characteristics, composition, topography, and weather. We have been doing comparative studies of dust events on Earth and Mars in order to shed light on important physical processes of the weather and climate of both planets. Our 2002 field campaign showed that terrestrial dust devils produce heat and dust fluxes two and five orders of magnitude larger than their background values. It also showed that charge separation within terrestrial dust devils produces strong electric fields that might play a significant role in dust sourcing. Since Martian dust devils and dust storms are stronger and larger than terrestrial events, they probably produce even stronger fluxes and electric fields. *INDEX TERMS:* 0343 Atmospheric Composition and Structure: Planetary atmospheres (5405, 5407, 5409, 5704, 5705, 5707); 0305 Atmospheric Composition and Structure: Aerosols and particles (0345, 4801); 0694 Electromagnetics: Instrumentation and techniques; 3307 Meteorology and Atmospheric Dynamics: Boundary layer processes; 3304 Meteorology and Atmospheric Dynamics: Atmospheric electricity; *KEYWORDS:* aerosol, convection, dust devil

Citation: Renno, N. O., et al. (2004), MATADOR 2002: A pilot field experiment on convective plumes and dust devils, *J. Geophys. Res.*, *109*, E07001, doi:10.1029/2003JE002219.

1. Background

[2] The concentration of atmospheric aerosol particles has increased significantly with human activity. Indeed, there are suggestions that the global aerosol climate forcing might be as large as a factor of two of the direct forcing due to greenhouse gases, and that regionally aerosol forcing can be even larger [*Climate Change*, 2001]. Aerosols produce a direct radiative forcing by scattering and absorbing solar and infrared radiation, and an indirect radiative forcing by altering cloud processes via increases in cloud droplet number and ice particle concentration. This effect increases the cloud albedo [*Twomey*, 1974] and can decrease the precipitation efficiency of terrestrial clouds [*Albrecht*, 1989]. Since human activity has been producing strong changes in the concentration of atmospheric aerosols, it is extremely important to understand the effects of aerosols on terrestrial weather and climate. We have been studying the direct effects of mineral dust on terrestrial weather and climate while developing techniques to probe Martian weather systems.

[3] The main objective of the Martian ATmosphere And Dust in the Optical and Radio (MATADOR) 2002 field campaign was to quantify the intensity and variability of the contribution of coherent plumes and convective vortices to the flux of heat and desert aerosols. Our observations showed that the heat transport by coherent convective

[1]Atmospheric, Oceanic and Space Sciences, University of Michigan, Ann Arbor, Michigan, USA.
[2]Lunar and Planetary Science Laboratory, University of Arizona, Tucson, Arizona, USA.
[3]Department of Environmental Sciences, Wageningen University, Wageningen, Netherlands.
[4]Space Physics Laboratory, University of California Berkeley, Berkeley, California, USA.
[5]NASA Goddard Space Flight Center, Greenbelt, Maryland, USA.
[6]Instituto del Medio Ambiente y el Desarrollo, Sustentable del Estado de Sonora (IMADES), Hermosillo, Mexico.
[7]Instituto Tecnologico de Sonora (ITSON), Ciudad Obregón, Mexico.
[8]Rincon Research Corporation, Tucson, Arizona, USA.
[9]Optech Corporation, Toronto, Ontario, Canada.

0148-0227/04/2003JE002219

plumes and dust devils is respectively more than one and two orders of magnitude larger than the background fair weather value, and that they produce even larger perturbations in the flux of dust. This result is consistent with measurements of large vertical transport of aerosols by dust devils over the US Southwest [*Gillette and Sinclair*, 1990] and tracer species by convective vortices over the boreal forest [*MacPherson and Betts*, 1997]. Convective vortices are extremely efficient in transporting heat and tracer species because their rotation produces a dynamic stability that inhibits mixing. This leads to large buoyancies, strong vertical velocities, and large concentration of tracers inside them.

[4] The two Viking Orbiters, Mars Global Surveyor (MGS), and Mars Odyssey (MO) showed that Aeolian processes in the form of wind erosion features, dust devils, and dust storms have been actively modifying the surface of Mars. The MGS also detected orbit-to-orbit variations in atmospheric density by factors of two or more at an altitude of 124 km, probably caused by variations in atmospheric dust content and temperature. Thus a better characterization of Martian dust devils and dust storms is important for the understanding of some of the most important processes actively modifying the Martian surface, and producing short-term atmospheric variability that affects aerobraking and aerocapture.

[5] There is evidence that, besides dust storms, dust devils play an important role in the Martian dust cycle. This idea is consistent with the fact that the atmospheric dust opacity increased throughout the Mars Pathfinder (MPF) mission in spite of low wind conditions and the absence of dust storms on the planet. Indeed, *Ferri et al.* [2003] showed that the dust flux due to dust devils on an active Martian day is an order of magnitude larger than the mission-mean deposition rate observed at the MPF landing site. This result confirms that dust devils contribute significantly to the maintenance of dust in the atmosphere of Mars, perhaps even being the primary suppliers of dust into the atmosphere of the Ares Vallis region.

[6] On Mars, dust devils are much bigger and stronger than on Earth. Terrestrial dust devils have typical diameters of less than 10 m and are seldom higher than 500 m [*Sinclair*, 1973]. In contrast, dust devils with diameters between 100 m and 1 km, and heights in excess of 5 km are frequently observed on Mars [*Thomas and Gierasch*, 1985; *Malin et al.*, 1999]. However, even small terrestrial dust devils can be dangerous to aviation. There are reports that up to 10% of the accidents with light aircrafts, sailplanes, helicopters, and blimps are caused by wind gusts associated with dry convection and dust devils [*Spillane and Hess*, 1988]. Charged dust particles produce electrical fields in excesses of 10 kV/m in terrestrial dust devils [*Farrell et al.*, 2002, 2003; *Krauss et al.*, 2002]. Martian dust devils have higher dust content and may produce even stronger electrical fields. The dust devils observed in the Pathfinder images have about 700 times the dust content of the local background atmosphere [*Metzger et al.*, 1999]. Thus electrically charged Martian dust devils and dust storms are potential hazards to Landers and will be dangerous to future astronauts exploring its surface. Indeed, the design of adequate mechanical and electrical systems for these Landers cannot progress effectively without a better understanding of Martian dust devils and dust storms. Moreover, ancillary phenomena associated with electrically charged vortices can ionize atmospheric gases and might have important implications for atmosphere chemistry.

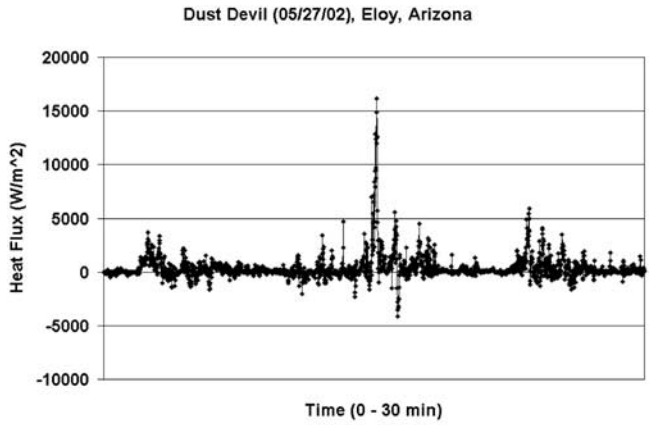

Figure 1. Surface sensible heat flux (from 10 Hz eddy correlation measurements at 3 m above the surface) for a 30 min interval.

2. Theories and Hypotheses

[7] During the 2002 MATADOR experiment we found that the heat and dust fluxes in terrestrial convective plumes and dust devils can be many orders of magnitude larger than their background values of a few 100 W/m^2 and a few 100 $\mu g/m^2$ s (see Figure 1 and *Gillette and Sinclair* [1990]). We hypothesize that dust devils are also a significant source of atmospheric dust in most of the Martian landscape. During the 2002 experiment, we discovered correlated fluctuations in convective activity and atmospheric opacity. We hypothesize that these fluctuations are caused by a feedback between convective activity and atmospheric dust loading. In addition, we observed that intense convective circulations such as dust devils and convective plumes are more frequent in regions of large horizontal temperature gradients. We suggest that this happens because temperature gradients caused by surface heterogeneities produce baroclinic vorticity and force anomalously high sensible heat fluxes. Finally, we observed that contact electrification between colliding dust particles produces strong electric fields in dust devils. These strong electric fields are consistent with the suggestion by *Renno et al.* [2003] that micro-discharges between colliding dust particles produce nonthermal microwave emission. Below, we summarize the theoretical framework that we have been using for guiding and interpreting our field observations.

2.1. A Scaling Theory for Convective Plumes and Dust Devils

[8] The properties of convective circulations such as those produced by convective plumes and vortices can be calculated with the theories proposed by *Renno and Ingersoll* [1996] and *Renno et al.* [1998, 2000]. According to their

theories, the bulk pressure drop from the ambient to the center of a convective plume or vortex is a measure of their intensity. The theory shows that the bulk pressure drop across a convective circulation is given by

$$\Delta p \equiv (p_\infty - p_o) \approx p_\infty \left\{ 1 - \exp\left[\left(\frac{\gamma\eta}{\gamma\eta - 1} \right) \left(\frac{c_p}{R} \right) \left(\frac{\Delta T}{T_\infty} \right) \right] \right\}, \quad (1)$$

where p_o is the surface pressure at the plume or vortex center, p_∞ and T_∞ are the surface pressure and temperature at a large radial distance from their center, γ is the fraction of the total dissipation of mechanical energy consumed by friction near the surface, η is the thermodynamic efficiency, c_p is the atmospheric specific heat capacity at constant pressure, R is the atmosphere's gas constant, and ΔT is the effective temperature perturbation (defined by equation (4) below). The maximum thermodynamic efficiency of a heat engine is $\eta = (T_h - T_c)/T_h$, where $T_h \approx T_\infty$ and T_c are, respectively the entropy-weighted mean temperatures of the regions where heat is absorbed (the surface air) and where rejected (the troposphere). For a dry convective layer, $\eta = \Gamma_d Z/T_h$, where Γ_d is the dry adiabatic temperature lapse-rate and Z is the depth of the convective layer [*Souza et al.*, 2000].

[9] It follows from equation (1) that the pressure drop across a typical convective plume or vortex (i.e., when $\eta \ll 1$ and $\Delta p/p_\infty \ll 1$) can be approximated by

$$\Delta p \approx \frac{\gamma\eta c_p p_\infty \Delta T}{R T_\infty}. \quad (2)$$

Equation (2) shows that the intensity of a convective plume depends on its depth (via its thermodynamic efficiency) and the value of its temperature perturbation. The existence and size of a convective vortex, in turn depends on the presence of vorticity and its magnitude [*Renno and Bluestein*, 2001]. As air parcels move toward the center of the updraft in the presence of vorticity, they spin while attempting to conserve angular momentum. To a first approximation, the wind around a small convective vortex (Rossby number $\gg 1$) is in cyclostrophic balance; that is, the pressure gradient force balances the centrifugal force. Surface friction reduces the angular momentum of spinning air parcels moving toward the center of the vortex and perturbs the balance between centrifugal and pressure gradient forces. The decrease in the centrifugal force makes the near surface air to converge toward the vortex center. When dust is entrained into the rising vortex, it becomes a dust devil. Assuming cyclostrophic balance, and using equation (2) and the ideal gas law, we find that the maximum tangential wind speed around a small vortex is

$$v_a \approx \left(\frac{\gamma\eta c_p \Delta T}{p_\infty} \right)^{\frac{1}{2}}. \quad (3)$$

Equation (3) shows that the wind speed around a convective vortex depends only on the thermodynamics of its convective heat engine; that is, it does not depend explicitly on the mechanisms responsible for the generation of vorticity. However, the vortex size is proportional to the value of the background vorticity [*Renno and Bluestein*, 2001]. For larger convective vortices such as regional or synoptic scale weather systems, the wind speed must be determined from the assumption of gradient or geostrophic balance.

[10] *Renno and Ingersoll* [1996] show that the product of the buoyancy with the distance over which it does work on rising air parcels is equal to the energy available for a unit mass air parcel to do work, $W = \eta\, c_p\, \Delta T$. They used this idea and the Newtonian cooling approximation to show that the maximum temperature fluctuation associated with convective plumes over homogeneous surfaces is

$$\Delta T \approx \left(\frac{c_p \eta F_{in}}{8\varepsilon\sigma_R g H T_c^2} \right), \quad (4)$$

where F_{in} is the surface heat flux; ε is the atmosphere's emissivity; σ_R is the Stefan-Boltzmann constant; g is the gravity acceleration; and H is the depth of the convective layer.

[11] *Souza et al.* [2000] show that the intensity of convective circulations forced by surface inhomogeneities in sloping terrains depends on the near-surface nonadiabatic temperature difference across the ascending and descending branches of the circulation and the depth of the convective layer. In this case, ΔT is given by

$$\Delta T = \Delta T_{ac} - \Delta T_{ad} = \Delta T_{ac} - \Gamma_d \Delta_z, \quad (5)$$

where the subscripts *ac* and *ad* stand for actual and adiabatic, $\Delta T_{ad} = \Gamma_d\, \Delta z$ is the temperature drop following a dry adiabat, and Δz is the difference in elevation between the ascending and descending branches of the circulation. This result is consistent with observations that intense convective circulations such as dust devils and convective plumes are more frequent in regions of large temperature gradients or sloping terrains.

[12] When the surface is composed of loose materials, dust particles might become airborne making convective plumes and dust devils visible. These convective systems have the potential to transport large quantities of dust from the surface all the way to the top of the convective layer. Saltation is the mechanism by which dust is typically lifted from the surface [*Bagnold*, 1941]. During saltation sand grains move in a skipping motion that propels dust particles a few microns in diameter into the air. Bagnold's study allows the computation of the minimum friction wind speed necessary to initiate saltation

$$v^{*3} \approx A\left(\frac{\sigma g \nu}{\rho} \right), \quad (6)$$

where $A \approx 1.2 \times 10^{-2}$ is a nondimensional constant that depends on the angle of repose and the terrain slope, σ is the sand-grain density, g the planet's gravity acceleration, ν the kinematic viscosity of the air, and ρ is the air density. *Csanady* [1967] derived a simple relationship between the friction and free-stream wind by assuming that it joins the frictional boundary layer through a logarithmic velocity

profile. Csanady concluded that the free-stream wind speed necessary to initiate saltation is

$$v \approx \frac{v^*}{\sqrt{C_D}}, \quad (7)$$

where C_D is the surface's drag coefficient. According to *Bagnold* [1941] C_D ranges from 5×10^{-4} for a smooth surface to 1.5×10^{-3} for a rough surface. Thus we expect the free stream wind speed around "dusty" convective plumes and dust devils to depend on the availability of dust and the surface properties. This idea is consistent with the more precise experimental values obtained in wind tunnels [*Greeley et al.*, 1980; *Greeley and Iversen*, 1986; *White et al.*, 1997]. Equations (3) and (7) can be used to predict the possibility of saltation around a convective vortex. Saltation occurs whenever $v \geq v_a$.

2.2. Electric Fields

[13] Triboelectric charging of saltating and colliding dust particles produces bulk electrical fields well in excess of 10 kV/m in terrestrial dust devils [*Farrell et al.*, 2002; *Krauss et al.*, 2002; *Towner et al.*, 2002; *Farrell et al.*, 2003, 2004]. Since Martian dust devils are larger and stronger than their terrestrial analogues [*Thomas and Gierasch*, 1985; *Renno et al.*, 2000; *Cantor et al.*, 2002], it is likely that they produce stronger electrical fields and, perhaps even large-scale electrical discharges. Measurements in dust devils and dust storms show negative charges aloft, which is consistent with the idea that negative charges are transferred to the smaller dust particles during collisions [*Ette*, 1971; *Melnik and Parrot*, 1998]. Assuming that the larger particles stay in the saltation layer, while the smaller particles are lifted by the dust devil updrafts we can estimate the electric field generated by them.

[14] The maximum charge of airborne dust particles can be calculated by assuming that, after energetic collision between dust and sand particles during saltation, the particles' charging is limited by field emission [*Bernhard et al.*, 1992]. Then, a microdischarge occurs while the particles move away from each other and they are left with a residual charge of the order of that necessary to produce electric discharges [*Renno et al.*, 2003]. The negatively charged dust particles of a few μm in diameter then rise with the updraft producing the bulk electric fields observed in terrestrial dust devils, while the larger positively charged sand particles stay in the saltation layer. Then, knowing the dust particle concentration and the dust devil size, we can calculate the maximum electric field generated by them. In addition, we can calculate the atmospheric charging rate (current per unit area) produced by them by knowing the dust flux. Next, we do these order-of-magnitude calculations and compare the results with the observed electric fields reported in section 3.

[15] It follows from the calculations of *Renno et al.* [2003] that the residual charge in terrestrial dust particles of ~10 μm of radius is $q_{res} \sim 3 \times 10^{-15}$ C. This value is consistent with the results of laboratory experiments reported by *Bernhard et al.* [1992] and the observation of dust particles with charges of up to 10^{-12} C in terrestrial dust devils [*Farrell et al.*, 2004]. Terrestrial dust devils have dust concentrations $n_p \sim 10^7$ particles/m^3 and dust fluxes $F \sim 10^8$ particles/m^{2}s [*Renno et al.*, 2003]. Thus they have maximum charge densities of $\sim 10^{-8}$ C/m^3 and can produce vertical currents $I \sim 10^{-7}$ A/m^2. Approximating a dust devil by a cylinder of radius R and height H, we find that it can produce a near surface electric field given by

$$E_r \sim \left(k\pi R^2 n_p q_{res} H\right) / \left[r\left(r^2 + H^2\right)^{1/2}\right], \quad (8)$$

where $k = 9 \times 10^9$ N m^2/C^2 is Coulomb's constant, and r (>R) is the distance from the center of the dust devil. It follows from equation (8) that the electric field near the boundary (at $r \sim R$) of a typical dust devil of $H \sim 100$ m is $E \sim 0.1 \times R^2$ kV/m, where R is in meters. Thus a strong dust devil of radius $R \sim 10$ m produces a maximum near surface electric field of ~10 kV/m. This electric field is of the order of that reported in section 3.5 for a dust devil of radius $R \sim 7$ m. Thus the predictions of our simple model are consistent with observations of terrestrial dust devils. However, we still do not have simultaneous measurements of dust concentration, dust charge, and electric field in dust devils. These measurements would allow us to test our model and assumptions.

Table 1. Characteristics of the Sensor and Instruments Used in the 2002 MATADOR Field Campaign

Measurement	Instrument	Accuracy	Response Time
Pressure	Vaisala CS105	0.5 hPa	<1 s
Temperature	Vaisala HMP45C	0.5 K	<1 s
Humidity	Vaisala HMP45C	5% RH	~15 s
E-C temperature	Campbell CSAT3	0.1 K	<0.05 s
E-C humidity	Campbell KH2O	0.5%	0.01 s
E-C humidity	LiCor 7500	0.5 g/m^3	<0.05 s
E-C wind velocity	Campbell CSAT3	0.04 m/s	<0.05 s
Solar radiation	Kipp & Zonen CNR1	10%	<18 s
Infrared radiation	Kipp & Zonen CNR1	10%	<18 s
Soil heat flux	TNO Plates	10%	<10 s
Infrared soil temperature	Everest Infrared Thermometer	0.5 K	20 ms
Soil temperature	Soil PT100	0.3 K	<10 s
Electric field	Mission Instruments EFS1000 Field Mill	1%	0.1 s
Dust backscatter	Optech Lidar	5%	<1 s

3. Instruments and Observations

[16] Our field campaign site is located at the Santa Cruz Flats (32°40.319′N, 111°32.641W, 526 m of elevation) near Eloy, Arizona. This is a region of intense boundary layer convection and large dust devil activity. In order to achieve our objectives, we measured surface fluxes of heat, water vapor, short and long wave radiation, soil heat flux, pressure, wind, temperature, water vapor and dust concentration, as well as electric field. A list of the sensors used in our field campaign, as well as their accuracy and response time is displayed in Table 1.

[17] The fluxes of heat, dust, and water vapor were measured using eddy correlation. Eddy correlation is a micrometeorological technique for directly measuring turbulent fluxes in the atmospheric boundary layer. This method involves fewer assumptions than any other method. The heat flux is computed as the product of the heat capacity of air and the covariance between vertical wind

Figure 2. Typical "dusty" nonrotating convective plume (top left), pair of dust devils at the boundary between dry and irrigated fields (top right), and large dust devil (bottom left) observed during the MATADOR field campaigns. The big dust devil is about 200 m behind the truck near the center of the image at the bottom left. The MATADOR field site is located below the wingtip of the aircraft in the image at the bottom right. These pictures were taken by N. Renno during the MATADOR Field Campaigns.

velocity and air temperature fluctuations. The flux of tracer species such as water vapor is calculated as the product of the covariance between the vertical wind velocity and fluctuations of the water vapor content. *Kaimal and Businger* [1970] were the first to probe a dust devil with eddy correlation instruments. An in-depth discussion of the eddy-correlation technique and its theoretical basis is given by *Kaimal* [1975], *Businger* [1986], and *Lenschow* [1986]. The aerosol concentration inside a few dust devils was estimated with a lidar, and the electric fields were measured with field mills.

3.1. Effects of Rotation on Heat and Dust Fluxes

[18] An interesting result of the 2002 field campaign was the observation that the heat transport by coherent convective plumes and dust devils are respectively more than one and two orders of magnitude larger than the background fair weather value. Figure 1 shows the "eddy-correlation heat flux" measured during the passage of a group of three coherent plumes over our sensors. The central plume had a large dust devil (located at the center of the plot) with peak vertical velocity of almost 10 m/s (not shown). The peak sensible heat flux was in excess of 15 kW/m^2. Convective vortices are extremely efficient in transporting heat and tracer species because dynamic stability caused by rotation prevents mixing. This leads to large buoyancy, strong vertical velocity, and large concentration of tracers inside them. The stability of rotating fluids roots on the conservation of angular momentum. When a unit mass fluid parcel rotating with angular velocity ω is perturbed and acquires a velocity v in a direction perpendicular to its axis of rotation, the parcel is deflected by an acceleration of magnitude $2\omega v$. Thus the disturbed fluid parcel moves on a circular path of radius r such that $v^2/r = 2\omega v$. Then, it goes around a circle of radius $r = v/2\omega$ that decreases with increases in the fluid's angular velocity and periodically returns to its original position (twice for every rotation of the fluid). This is the physical reason why rotation inhibits mixing. The transport of dust by convective plumes and vortices might be even stronger than the heat transport, but unfortunately good instruments for directly measuring the surface flux of dust were not available at the time of the MATADOR field experiments and we only estimated the order-of-magnitude of the dust flux. The dust concentration inside strong dust plumes and dust devils was about 0.1 g/m^3. The dust flux can be obtained by multiplying the dust concentration by the vertical velocity in the dust plumes and dust devils. Thus the dust flux in strong dust plumes and dust devils are, respectively of the order of 0.1 g/m^{2}s and 1 g/m^{2}s (see section 3.4).

[19] Figure 2 shows typical "dusty plumes" and dust devils observed during the MATADOR field campaigns. It also shows an aerial picture of our field test site during a day of shallow cumulus clouds and light winds (the field site is just below the aircraft's wingtip). Note that the atmosphere was quite dusty when the picture was taken. The frequency of the "dusty plumes" observed in Figure 2 is correlated with the oscillations in surface temperature and heat budget described in section 3.3.

3.2. Effects of Surface Heterogeneities on Convection

[20] Our observations show that convective plumes and vortices are more frequent in regions of large horizontal

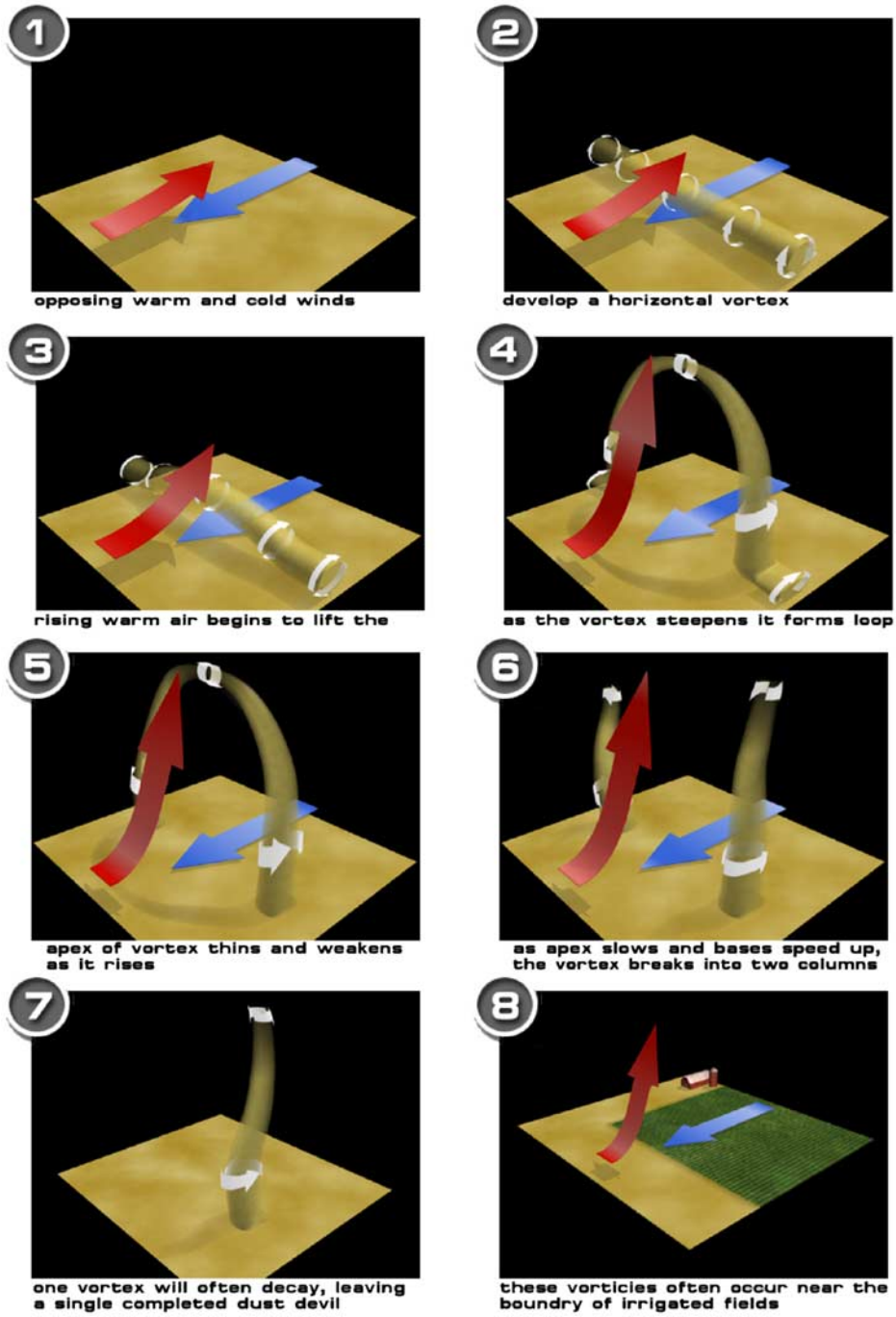

Figure 3. Sketch of a physical model for the formation of pairs of convective vortices near the boundary between cold and warm air masses. Courtesy of the University of Michigan.

temperature gradients such as that shown on the top-right corner of Figure 2. It follows from the second law of thermodynamics that the surface heat flux is proportional to the temperature difference between the ground and the near-surface air. A convecting air parcel absorbs heat from the surface while moving toward the updraft. Over flat terrain, an air-parcel temperature increases as it moves toward the updraft. Thus, when the ground temperature is uniform (no horizontal gradients), the surface heat flux decreases as an air parcel moves toward the updraft. However, in the presence of horizontal temperature gradients, the surface heat flux decreases less rapidly when an air parcel moves toward the warmer terrain. Moreover, horizontal temperature gradients lead to the baroclinic generation of vorticity. The presence of intense convection and vorticity leads to the genesis of an anomalously large number of convective vortices in these regions. This idea is illustrated in Figure 3. Both our theoretical model for dust devils and our physical explanation for their genesis are consistent with the results of numerical simulations of terrestrial and Martian dust devils [*Kanak et al.*, 2000; *Toigo et al.*, 2003]. In summary, our theory

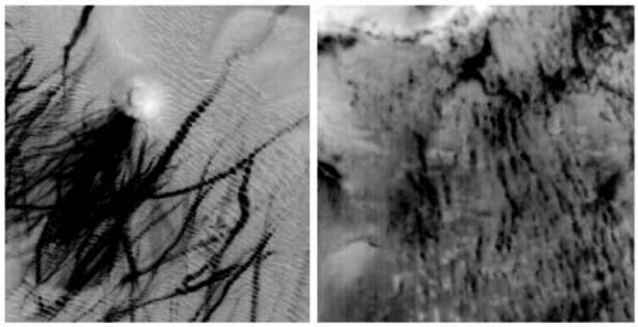

Figure 4. MOC narrow-angle (NA) and wide-angle (WA) camera. Images of dust devil tracks showing that groups of tracks seen in the NA images are also detected by the WA images. Thus groups of dust devil tracks seem to be associated with topography. Courtesy of NASA/JPL/Malin Space Science System.

suggests that heterogeneous surfaces have the potential of producing more intense convective circulations and a larger number of convective vortices than do homogeneous surfaces.

[21] Our theory also explains why sloping terrains force convective circulations (e.g., valley-mountain circulations). When topographical features are present, an air-parcel moving upslope cools down while expanding. Thus, when the temperature of a mountain slope decreases less rapidly with height than the dry adiabatic lapse rate, an air-parcel will continue absorbing heat while moving upward along the slope. Indeed, it is well known that, even for the same solar heat flux, the radiative-convective equilibrium temperature of the atmosphere over elevated terrains is higher than that in the free atmosphere over lower regions. That is, the temperature of a mountain slope decreases less rapidly with height than the dry adiabatic value and forces an anomalous large surface heat flux. Then, the depth of convective boundary layers becomes larger over mountains because of the anomalously high heat flux into upslope moving convective updrafts. Therefore topographical features enhance the strength of convective circulations by increasing both the heat input and the thermodynamic efficiency of the convective heat engine [see *Souza et al.*, 2000]. This might explain enhanced dust devil tracks downwind of Martian craters as shown in Figure 4.

3.3. Dust-Radiation Feedbacks

[22] Another interesting result of the MATADOR field experiment was the discovery of strong oscillations in the surface heat flux and the intensity of boundary layer convection with timescale of about a half hour (Figure 5). We hypothesize that these oscillations are due to the interaction between atmospheric convection, airborne dust and solar radiation. Intense boundary layer convection produces increases in the concentration of atmospheric dust. Then, airborne dust absorbs and scatters solar radiation producing a decrease in surface temperature and stabilizing the atmosphere. This, in turn, produces decreases in the intensity of atmospheric convection and dust flux. The $^1/_2$ hour timescale is of the order of the convective timescale. Indeed, it is the timescale that takes boundary layer convection to disperse the dust plume and intensify again.

3.4. Lidar Signature

[23] Two lidar systems from Optech Incorporated were employed during the 2002 field campaign. The two lidars were configured such that most of the measurements were performed in a horizontal direction with the beam approximately 1.5 m above the surface. However, measurements with one of the lidars were made at several different slant angles to probe the vertical structure of dust devils. The first lidar (L1) is a modified ceilometer based on a pulsed laser operating at a wavelength of 1.06 μm with output energy of about 15 mJ/pulse. This system was operated in a single pulse mode and mounted on a tripod with azimuth and elevation motions. A sighting scope for aiming was fixed to the lidar enclosure and co-aligned with the laser beam. This arrangement permitted visual location and manual tracking of dust devils. The return signal intensity from t_0 to the loss of signal was transferred to the laptop and stored for further analysis. The line-of-sight range resolution of this system was approximately 60 cm. The second lidar (L2) is a modified Optech Intelligence Laser Ranging and Imaging System (ILRIS) based on diode-pumped pulsed Erbium-glass laser operating at a wavelength of 1.535 μm (eye-safe) with a firing rate of 2000 Hz and low energy (5 μJ/pulse). This instrument is designed to provide rapid surveys of a region with programmable horizontal and vertical scan angles to provide a 3-D image of the reflecting targets. A video camera is incorporated in this instrument for aiming and defining the area to be scanned.

[24] Figure 6 shows two scans taken with L1 through a dust devil. The first scan was taken in the horizontal direction and the other with the beam at a slant angle of about 4 deg taken 30 s later. Near the surface the dust devil has a clear core, but at 100 m above the surface it has uniform dust content. These observations are consistent with our theoretical framework that predicts the maximum pressure drop at the surface.

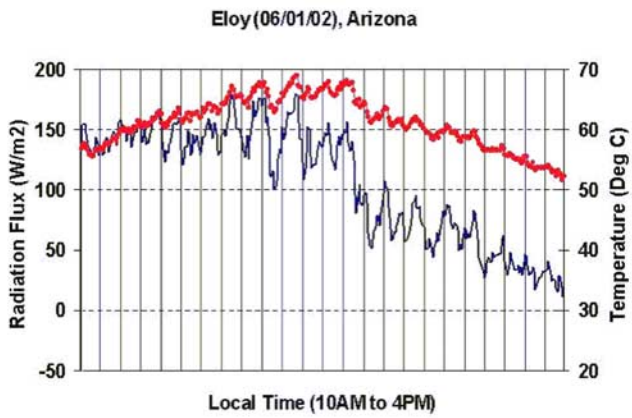

Figure 5. Ground temperature (red) and soil heat flux (blue). Note the oscillations with a timescale of about a half hour (the vertical lines are at 15 min intervals). These measurements were made during a day in which clouds were not present.

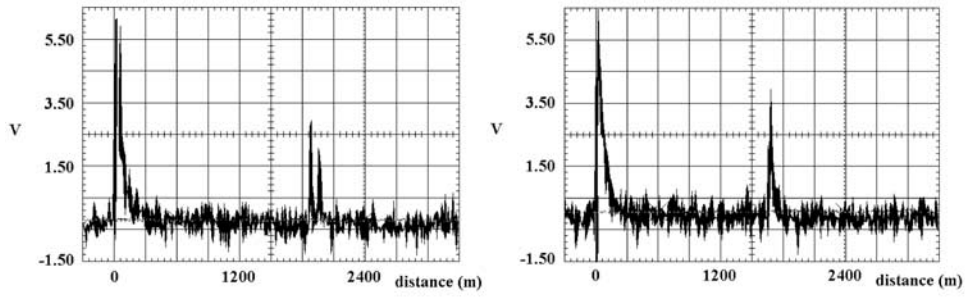

Figure 6. Lidar scans through a dust devil at about 2 m above the surface (left) and at about 100 m above the surface (right). Distance from the lidar is displayed on the horizontal axis, and the voltage output from the detector is displayed on the vertical axis.

[25] An analysis of the data obtained at 100 m above the surface was carried out in order to estimate the density of dust particles inside the dust devil relative to the local background value. The ratio of the dust density inside and outside the dust devil is approximately given by

$$\frac{n_2}{n_1} \cong \frac{(r_2)^2 P_2[1+2\beta_1 r_2]}{(r_1)^2 P_1[1+2\beta_1 r_1]} \tag{9}$$

where the subscripts i = 1 and 2 refer to measurements outside and inside the dust devil, n_i is the dust density, r_i is the range of the observed lidar signal, P_i is the observed lidar backscattered signal, and β_1 is the extinction at 1.06 μ, given by the product n σ_s, where σ_s is the dust scattering cross-section. A first order calculation of the relative density was carried out assuming β is equal to 6.36×10^{-2}/km for a rural aerosol model with 50% relative humidity [*Shettle and Fenn*, 1979]. The results of these calculations indicate the relative dust density to be of the order of 10^3.

[26] Since the dust content inside the dust devil whose scan is presented in Figure 6 is 10^3 times the background value of $\sim$100 μg/m^3 [*Metzger et al.*, 1999], we find the that its dust concentration is $\sim$0.1 g/m^3. The peak dust concentration inside a dust devil times the peak vertical velocity in its interior gives the peak bulk dust flux. We assume that dust plumes have similar dust concentration as dust devils, and calculate the dust flux in dust plumes and dust devils using their peak vertical velocities (1 and 10 m/s) measured with the sonic anemometer. This resulted in dust fluxes in strong dust plumes and dust devils of 0.1 g/m^{2}s and 1 g/m^{2}s, respectively.

[27] Figure 7 shows the dust distribution in a horizontal slice through a dust devil taken with L2. The variability of the internal structure is clearly seen in the filamentary variations of the image. The L2 lidar is located at the bottom of the picture and the image extends out to about 50 m from it. This lidar system does not record the full range-dependent signal return on each pulse; it only provides a single range measurement from the lidar to a target whose backscattered signal exceeds an instrument defined threshold value. Thus on each pulse only a single data point is recorded. Each data point accurately (with a line-of-sight resolution of 1 cm) locates the point where the reflected signal reaches the detection threshold level. It shows distinct structures in the dust devil eyewall.

3.5. Electrical Fields

[28] Our electrical fields measurements in terrestrial dust devils showed that they maintain tremendous charge separation and that their electric fields exceeds the breakdown potential ($\sim$10 kV/m) of the Martian atmosphere. Typical Martian dust devils would be up to 100 times larger and much stronger than their small terrestrial cousins. Thus strong charge separations and electric field breakdown are likely to occur on Mars. Figure 8 shows a ten minute period of the atmospheric electric field measured with a field mill during the 2001 field campaign. This data is similar but of better quality (less noisy) than the data collected during the 2002 field campaign [see *Farrell et al.*, 2003]. The broad event centered at 4 minutes corresponds to six small dust devils that were rotating together around a common center. The zero on the timescale corresponds to about 3 pm local time. The group of dust devils passed by the instrument moving south then turned easterly, effectively bending around the site. This explains the unusual width of the signal. The closest approach was about 10–15 meters away from the sensor. The large peak centered at about 5.5 minutes was produced by a dust devil of approximately 7 m in diameter

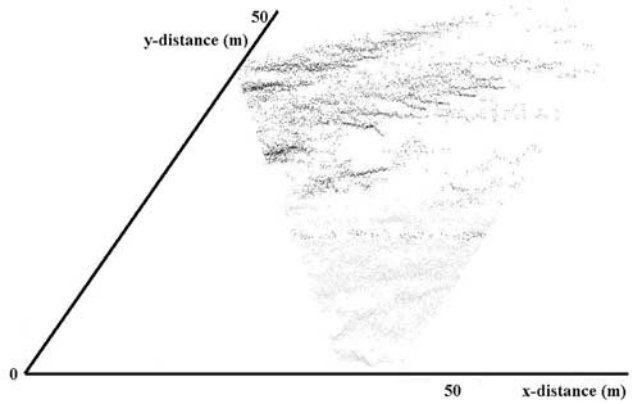

Figure 7. Horizontal slice through a dust devil measured with L2. Each point in the image represents the location in which the lidar backscatter first reaches a predefined threshold value.

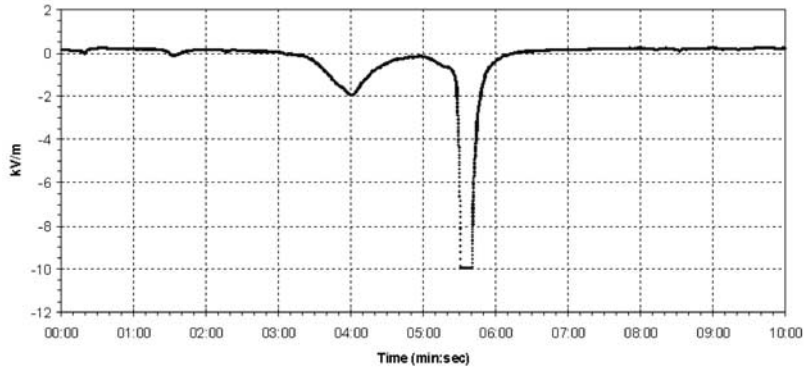

Figure 8. Electric field measured by a field mill during the passage of dust devils.

that passed directly over our instruments and moved without changing direction. The field mill was pegged at its maximum value for about 9 seconds. The observed electric field is consistent with the predictions of the simple model described in section 2.2. The model predicts that a strong dust devil of radius R $\sim$ 10 m produces a maximum near surface electric field of $\sim$10 kV/m. However, we would need simultaneous measurements of dust concentration, dust charge, and electric field near dust devils to test our model and the validity of all assumptions. More detailed discussion of the electric field measurements is presented in an article by *Farrell et al.* [2004].

4. Conclusions

[29] The MATADOR project was designed to study the relationship between dynamical and electrical properties of terrestrial and Martian dust devils. Data collected during the 2002 field campaign in Arizona shows that convective plumes and dust devils play an important role in the vertical transport of heat and mineral dust. The data shows that dust devils produce heat fluxes two orders of magnitude larger than the background ambient flux, and even larger dust fluxes. Dusty convective plumes and dust devils are also an important source of atmospheric dust on Mars. Calculations reported in *Ferri et al.* [2003] show that dust devils observed on an active day pumped an order of magnitude more dust into the Martian atmosphere that the mean dust settling rate observed during the Mars Pathfinder mission. Our field campaigns also showed that charge separation within terrestrial dust devils produce electric fields in excesses of 10 kV/m. These electric fields might play a significant role on dust sourcing. Since Martian dust devils and dust storms are stronger and larger than terrestrial events, they probably produce even stronger electric fields. Thus Martian dust devils are important sources of atmospheric dust, produce strong electric fields, and are potentially harmful to spacecraft Landers and Rovers.

[30] The MATADOR field campaigns shed light on some of the basic physical processes operating in dust devils and dust storms. However, a fair amount of laboratory experiments, field research, and theoretical studies are still necessary for a complete understanding of these interesting weather phenomena. In order to quantify the contribution of terrestrial dust devils to atmospheric dust loading, we need measurements of the dust flux with a fast response sensor. In addition, we need simultaneous measurements of the atmospheric dust concentration, dust-settling rate, and frequency and fractional area covered by dust devils. In order to quantify the dust electrification and test our theoretical models, we need measurements of the dust particle concentration, dust flux, and electric field. We plan to complement our instruments with a new dust sensor and a scanning lidar to be able to accomplish these goals.

[31] **Acknowledgments.** The authors are very thankful to Francesca Ferri and Anthony Toigo for their thorough review and excellent suggestions. They also thank NASA HEDS, and the National Science Foundation for partially supporting this research under grant SGER 0225555.

References

Albrecht, B. A. (1989), Aerosols, cloud microphysics, and fractional cloudiness, *Science*, *245*, 1227–1230.

Bagnold, R. A. (1941), *The Physics of Blown Sand and Desert Dunes*, Methuen, New York.

Bernhard, A. K., K. Sattler, and H. C. Siegmann (1992), Gas breakdown in contact electrification, *J. Phys. D*, *25*, 139–146.

Businger, J. A. (1986), Evaluation of the accuracy with which dry deposition can be measured with current micrometeorological techniques, *J. Clim. Appl. Meteorol.*, *25*, 1100–1124.

Cantor, B., M. Malin, and K. S. Edgett (2002), Multiyear Mars Orbiter Camera (MOC) observations of repeated Martian weather phenomena during the northern summer season, *J. Geophys. Res.*, *107*(E3), 5014, doi:10.1029/2001JE001588.

Climate Change (2001), *Impacts, Adaptation and Vulnerability—Contribution of Working Group II to the Third Assessment Report of the Intergovernmental Panel on Climate Change (IPCC)*, 1000 pp., World Meteorol. Organ., Geneva.

Csanady, G. T. (1967), On the "resistance law" of a turbulent Ekman layer, *J. Atmos. Sci.*, *24*, 467–471.

Ette, A. I. I. (1971), The effect of Hermattian dust on atmosphere electric parameters, *J. Atmos. Terr. Phys.*, *33*, 295–300.

Farrell, W., et al. (2002), Quantification of charge in a dust devil based on its ULF magnetic signature, *Eos Trans. AGU*, *83*(47), Fall Meet. Suppl., Abstract P51A-0036.

Farrell, W. M., G. T. Delory, S. A. Cummer, and J. R. Marshall (2003), A simple electrodynamic model of a dust devil, *Geophys. Res. Lett.*, *30*(20), 2050, doi:10.1029/2003GL017606.

Farrell, W. M., et al. (2004), Electric and magnetic signatures of dust devils from the 2000–2001 MATADOR desert tests, *J. Geophys. Res.*, *109*, E03004, doi:10.1029/2003JE002088.

Ferri, F., P. H. Smith, M. Lemmon, and N. O. Rennó (2003), Dust devils as observed by Mars Pathfinder, *J. Geophys. Res.*, *108*(E12), 5133, doi:10.1029/2000JE001421.

Gillette, D., and P. C. Sinclair (1990), Estimation of suspension of alkaline material by dust devils in the United States, *Atmos. Environ.*, *24*, 1135–1142.

Greeley, R., and J. D. Iversen (1986), Aeolian processes and features at Amboy Lava Field, California, in *Physics of Desertification*, edited by F. El-Baz and M. H. A. Hassan, pp. 290–317, Martinus Nijhoff, Zoetermeer, Netherlands.

Greeley, R., R. Leach, B. White, J. Iversen, and J. Pollack (1980), Threshold windspeeds for sand on Mars: Wind tunnel simulations, *Geophys. Res. Lett.*, *7*, 121–124.

Kaimal, J. C. (1975), Sensor and techniques for direct measurement of turbulent fluxes and profiles in the atmospheric surface layer, in *Atmospheric Technology*, pp. 7–23, Natl. Cent. for Atmos. Res., Boulder, Colo.

Kaimal, J. C., and J. A. Businger (1970), Case studies of a convective plume and dust devil, *J. Appl. Meteorol.*, *9*, 62–620.

Kanak, K. M., D. Lilly, and J. Snow (2000), The formation of vertical vortices and the convective boundary layer, *Q. J. R. Meteorol. Soc.*, *126*, 2789–2810.

Krauss, C. E., et al. (2002), Laboratory experiments on electrostatic discharging in Martian dust devils and dust storms, *Eos Trans. AGU*, *83*(47), Fall Meet. Suppl., Abstract P51A-0338.

Lenschow, D. H. (1986), *Probing the Atmospheric Boundary Layer*, Am. Meteorol. Soc., Boston, Mass.

MacPherson, J. I., and A. K. Betts (1997), Aircraft encounters with strong coherent vortices over the boreal forest, *J. Geophys. Res.*, *102*, 29,231–29,234.

Malin, M. C., et al. (1999), Early views of the Martian surface from the Mars Orbiter Camera of Mars Global Surveyor, *Science*, *279*, 1681–1685.

Melnik, O., and M. Parrot (1998), Electrostatic discharge in Martian dust storms, *J. Geophys. Res.*, *103*(A12), 29,107–29,118.

Metzger, S. M., et al. (1999), Dust devil vortices seen by the Mars Pathfinder camera, *Geophys. Res. Lett.*, *26*, 2781–2784.

Renno, N. O., and H. B. Bluestein (2001), A simple theory for waterspouts, *J. Atmos. Sci.*, *58*, 927–932.

Renno, N. O., and A. P. Ingersoll (1996), Natural convection as a heat engine: A theory for CAPE, *J. Atmos. Sci.*, *53*, 572–585.

Renno, N. O., M. L. Burkett, and M. P. Larkin (1998), A simple thermodynamical theory for dust devils, *J. Atmos. Sci.*, *55*, 3244–3252.

Renno, N. O., A. A. Nash, J. Lunine, and J. Murphy (2000), Martian and terrestrial dust devils: Test of a scaling theory using Pathfinder data, *J. Geophys. Res.*, *105*, 1859–1865.

Renno, N. O., A.-S. Wong, S. K. Atreya, I. de Pater, and M. Roos-Serote (2003), Electrical discharges and broadband radio emission by Martian dust devils and dust storms, *Geophys. Res. Lett.*, *30*(22), 2140, doi:10.1029/2003GL017879.

Shettle, E. P., and R. W. Fenn (1979), Models for the aerosols of the lower atmosphere and the effects of humidity variations on their optical properties, *Environ. Res. Pap. 676*, Air Force Geophys. Lab., Lexington, Mass.

Sinclair, P. C. (1973), The lower structure of dust devils, *J. Atmos. Sci.*, *30*, 1599–1619.

Spillane, K. T., and G. D. Hess (1988), Fair weather convection and light aircraft, helicopters, and glider accidents, *J. Aircraft*, *25*, 55–61.

Souza, E. P., et al. (2000), Convective circulations induced by surface heterogeneities, *J. Atmos. Sci.*, *57*, 2915–2922.

Thomas, P. C., and P. J. Gierasch (1985), Dust devils on Mars, *Science*, *230*, 175–177.

Toigo, A. D., M. I. Richardson, S. P. Ewald, and P. J. Gierasch (2003), Numerical simulation of Martian dust devils, *J. Geophys. Res.*, *108*(E6), 5047, doi:10.1029/2002JE002002.

Towner, M. C., S. M. Metzger, T. J. Ringrose, M. Balme, R. Greeley, and J. C. Zarnecki (2002), Measurements of dust devil lower structure and properties, El Dorado Valley, Nevada, June 2002, *Eos Trans. AGU*, *83*(47), Fall Meet. Suppl., Abstract P51A-0342.

Twomey, S. (1974), Pollution and the planetary albedo, *Atmos. Environ.*, *8*, 1251–1256.

White, B., B. Lacchia, R. Greeley, and R. Leach (1997), Aeolian behavior of dust in a simulated Martian environment, *J. Geophys. Res.*, *102*(E11), 25,629–25,640.

V. J. Abreu, J. Koch, and N. O. Renno, Atmospheric, Oceanic and Space Sciences, University of Michigan, 2455 Hayward Street, Ann Arbor, MI 48109-2143, USA. (nrenno@umich.edu)

A. Carswell, Optech Corporation, Toronto, Ontario, Canada.

D. Burose, H. A. R. De Bruin, and O. K. Hartogensis, Department of Environmental Sciences, Wageningen University, Wageningen, Netherlands.

G. T. Delory, Space Physics Laboratory, University of California Berkeley, Berkeley, CA 94720, USA.

W. M. Farrell, NASA Goddard Space Flight Center, Greenbelt, MD 20771, USA.

J. Garatuza, Instituto Tecnologico de Sonora (ITSON), Ciudad Obregón, Mexico.

M. Parker, Rincon Research Corporation, Tucson, AZ, USA.

P. H. Smith, Lunar and Planetary Science Laboratory, University of Arizona, Tucson, AZ 85721, USA.

C. J. Watts, Instituto del Medico Ambiente y el Desarrollo, Sustentable del Estado de Sonora (IMADES), Hermosillo, Mexico.